

QUANTIFYING MIXING IN A CONVECTIVE BOUNDARY LAYER

Dore V.*, Moroni M. and Cenedese A.

*Author for correspondence

Department of Hydraulics, Transportations and Roads,
Sapienza University of Rome,
Via Eudossiana 18, 00184 Rome (Italy)
E-mail: valentina.dore@uniroma1.it

ABSTRACT

The phenomenon of penetrative convection in a stably stratified fluid has been reproduced in laboratory employing a tank filled with water and subjected to heating from below. The goal in the experiment is predicting the mixing layer growth as a function of initial and boundary condition and describe the fate of a tracer dissolved in the fluid phase. The equipment employed is suitable for simultaneously providing temperatures inside the domain through thermocouples (sensitivity less than 0.1 °C) and Lagrangian particle trajectories obtained by using a 2D image analysis technique named Feature Tracking. The field of view is illuminated through a thin light sheet with a suitable optical equipment. The mixing layer growth is detected both employing temperature data and statistics of the velocity field, i.e. the vertical velocity component variance. Concerning the transport feature of the phenomenon under investigation, the velocity spatial correlation allows the plume horizontal dimension to be determined. This information coupled to the knowledge of the mixing layer height allows the spatial extension of the convective region to be fully described.

INTRODUCTION

Penetrative convection is the motion of vertical plumes or domes into a fluid layer of stable density and temperature stratification providing the plumes have enough momentum to extend into the stable layer for a significant distance from the original interface. In its initial stages, the convective boundary layer is organized in coherent structures persisting over time. Subsequently the flow becomes turbulent and the structures break up.

Penetrative convection is of importance in several areas of geophysical fluid dynamics, most notably in the lower atmosphere, the upper ocean, and lakes, i.e. fluid bodies periodically stably stratified (their mean density decreases upwards) in most regions.

In most lakes, turbulent convective flow can be observed when the free surface becomes cooler than the underlying

waters, eroding the stable stratification on a daily or seasonal time scale [8].

In the ocean under calm conditions, the upper twenty or thirty meters usually exhibit a continuous, moderately stable density distribution. When wind begins to blow over the surface, turbulence in the water is generated both by shear and by sporadic breaking waves. With time, the turbulent layer becomes deeper as a result of the entrainment and erosion of the underlying denser water. Because of the relatively rapid mixing, the density distribution is approximately uniform in the upper layer, and the entrainment takes place across the interface between the turbulent and stable fluids [10].

An analogous phenomenon is observed in the atmosphere when surface heating due to solar radiation results in a growing unstable layer adjacent to the ground which replaces a nocturnal inversion from below. In this case, the initially stable environment near the ground is affected by convection, and full interaction between the two regions occurs [7][19].

In lakes and oceans, domes with large downward velocities are originating at the free surface, balanced by ascending domes with lower velocity but a larger area. In the atmosphere, the convection is characterized by relatively narrow plumes in the form of domes of rising horizontal surfaces balanced by larger regions of descending motion.

Resulting oscillatory movements (internal waves) generated within the stable layer take place at or below the Brunt-Väissälä frequency which is related to the vertical temperature gradient.

The dynamic of penetrative convection in nature influences the transport and mixing features of stratified fluids, in fact the flux through the interface between the mixing layer and the stable layer plays a fundamental role in characterizing and forecasting the distribution of chemical species with implication for:

- air or water quality (pollutants, released inside the mixing layer, are confined inside it)

- absorption of UV radiation (ozone, a natural filter for UV in the upper atmosphere, but a harmful contaminant in the lower troposphere)
- climate change (greenhouse gases)
- water turnover, ecosystems, algal blooms and eutrofization (oxygen and nutrients in oceans and lakes)

The combined use of thermocouples and flow visualization techniques allows the simultaneous measurement of temperature and velocity components. This then allows employing and cross-validating different methods to estimate the mixing layer height evolution with time. The feedback of this information to the characterisation of mixing will be shortly described.

Feature Tracking (FT) was used to reconstruct tracer particle trajectories because it is suitable for analyzing any particle density images and it does not require a known background flow or *a priori* velocity estimates to identify particles and their trajectories [22][4]. The technique employed for this investigation implements a pure translation model [14] [16]. FT algorithms focus their attention on pixel luminosity intensity gradients distributed within each image, recalling the “image brightness constancy constraint” and assuming the hypothesis of tracer particles behaving as Lambertian surfaces.

When studying turbulent convective phenomenon, dispersion is mostly due to transport by large organized structures while molecular diffusion can be neglected. The knowledge of the horizontal and vertical extension of the structures dominating the flow field appears to be mandatory. The vertical dimension is associated to the mixing layer height. In its calculation the entrainment has to be taken into account to carefully determine the upper limit a contaminant can reach. On the other hand, the spatial correlation of the velocity field, providing the plume horizontal dimension, allows the horizontal extension of the mixing region to be determined.

Another way of dealing with the dispersion topic is through the formulation of the transient turbulence theory. The main output of the theory is the transient matrix that accounts for all the mixing processes resolved by the grid spacing, from smallest eddy traced by the particles to the medium and large coherent structures over the entire mixed layer depth (for details see [1] and [17]).

NOMENCLATURE

β	[1/°C]	Thermal expansion coefficient
$1/\alpha$	[°C/cm]	Temperature gradient before heating starts
k	[W/cm °C]	Thermal conductivity
ν	[N cm s/kg]	Kinematic viscosity
g	[cm/s ²]	Gravity acceleration
\mathbf{x}_i	[cm]	Displacement vector
z	[cm]	Cartesian vertical direction
t	[s]	Time
u_i	[cm/s]	Velocity component along direction i
T	[°C]	Temperature
θ	[°C]	Potential temperature
q	[cm °C/s]	Kinematic heat flux
Δ		Interval

Upscripts	
*	Convective parameter scale
'	Parameter fluctuation part
-	Parameter mean part
Subscripts	
0	Reference for t=0
s	Surface
b	Bottom
c	Cold temperature
w	Warm temperature

EXPERIMENTAL SET-UP

The container, as shown in Figure 1, is a prismatic tank of square cross-section, 41x41x40 cm³. Its sidewalls are insulated by 3 cm thick polystyrene sheets. Insulation is maintained when the tank is filled with a density-stratified fluid but removed on the side facing the camera, to allow access for viewing. The working fluid is distilled water, rather than air (the similarity with the phenomenon occurring in the atmosphere still holds), to allow both a large heating rate and sufficient time to take measurements of the evolving thermal structure. A fluid density stable stratification within the test section, e.g. a positive vertical temperature gradient, is obtained employing the two tanks method. The fluid is initially equally distributed into two identical tanks set at the same height.

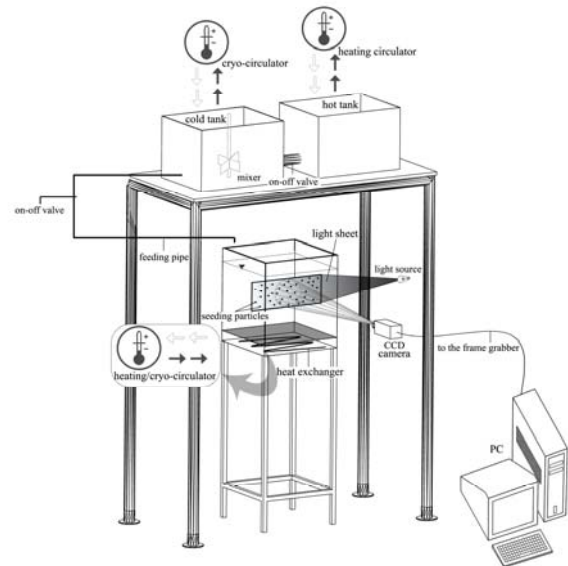


Figure 1 Experimental set up

Experiment #	T_{b0} (°C)	T_{bw} (°C)	$\alpha = (\partial z / \partial \bar{T})$ (cm/°C)
1	11	35	1.08
2	21	30	1.8

Table 1 Features of the experiments

The temperatures inside the tanks are initially set to: T_w (“warm” tank) and T_c (“cold” tank). A tube, connecting the “cold” tank and the test section, fills the latter with a temperature-stratified working fluid. In fact, the temperature

within the “cold” tank will increase with time because of the input of warm water caused by the head difference between the two tanks. An agitator is placed within the cold tank to homogenize the temperature inside. The temperature at the upper boundary is maintained at a constant value by an insulating polystyrene sheet. Water within the test section lower boundary is in contact with a circulating water bath connected to a cryostat, separated from the fluid by an aluminium sheet fitting the tank horizontal cross-section. During the filling procedure, the cryostat maintains the temperature of the lower boundary at a fixed value T_{b0} , approximately equal to the cold tank temperature. At the right time, the cryostat provides heat to start and sustain the phenomenon by maintaining a temperature always greater than the average temperature within the mixing layer. In fact, thermal convection is initiated upon replacing the cool water circulating under the lower boundary with warm water of temperature greater than the upper boundary temperature (time $t=0$). The temperature at the bottom, T_b , gradually increases approaching the final value, T_{bw} .

The initial fluid conditions are velocity equal to zero and the temperature increases with height with a continuous approximately linear trend of slope α .

Temperature was detected through thermocouples placed within the test section along a vertical line (array of 26 thermocouples) to measure vertical profiles and on the lower boundary to test horizontal homogeneity.

Velocity was detected through an image analysis technique (Feature Tracking). Images of well reflecting tracers (pollen particles with average size equal to about $d_p=80\ \mu\text{m}$) were recorded using a monochrome 8-bit CCD camera with a time resolution of 25 fps, focused on the mixing layer region (acquisition window of about 15 cm side). The fluid was seeded during the test section filling up. The measuring plane was illuminated by a thin light sheet obtained collimating a divergent light beam, produced by a 150 Watt halogen source, using a light-line guide equipped with a cylindrical lens.

The acquisition procedure can be divided into two steps: at first images are stored on the mass memory of a computer (576x764 pixels as resolution), next they are analyzed to detect trajectories.

DATA PROCESSING

Thermocouples provide the instantaneous values of temperature. When heating is started from below, the linear temperature profile associated to the stratification inside the domain starts to break up and change with time as far as the phenomenon evolves (Figure 2 for exp #1 and Figure 3 for exp #2). Vertical temperature profiles acquired during heating allow the measurement of the growth of the mixing layer with time ($z_i(t)$). Knowing the mean temperature within the mixing layer, $\bar{T}(t)$, the height can be calculated through the following relation:

$$z_i(t) = a(\bar{T}(t) - T_{b0}) \quad (1)$$

As mentioned before, the height of mixing layer is comparable with the domes vertical dimension. Starting from this idea we can evaluate the mixing layer height with a given

frequency (anyway less than 25 Hz, the largest frame rate for image acquisition) by dividing the domain into layers and computing the vertical velocity variance profiles (the horizontal homogeneity assumption allows averaging velocity data in each layer over a chosen time interval).

The horizontal extent of domes can be investigated through the spatial correlation of the velocity field, which is defined as follows:

$$\begin{aligned} R_{u'_i u'_j}(\mathbf{x}_1, \mathbf{x}_2, t) &= \overline{u'_i(\mathbf{x}_1, t) u'_j(\mathbf{x}_2, t)} \\ &= \int_{-\infty}^{\infty} \int_{-\infty}^{\infty} u'_i(\mathbf{x}_1, t) u'_j(\mathbf{x}_2, t) p(u'_i, u'_j, t) du'_i du'_j \end{aligned} \quad (2)$$

where the fluctuating part of each velocity component, u'_i and u'_j (if $i=j$ we obtain the autocorrelation function), are measured at points \mathbf{x}_1 and \mathbf{x}_2 and at time t , $p(u'_i, u'_j, t)$ is the joint probability density function. Setting $\mathbf{x}_1 = \mathbf{x}$ and $\mathbf{x}_2 = \mathbf{x} + \mathbf{r}$ it is

$$R_{u'_i u'_j}(\mathbf{x}_1, \mathbf{x}_2, t) = R_{ij}(\mathbf{x}, \mathbf{r}, t) \quad (3)$$

If the assumption of horizontal homogeneity is satisfied, the spatial correlation is only function of the distance r , of the height z and time t , i.e. $R_{ij}(z, r, t)$.

TRENDS AND RESULTS

Vertical temperature profiles acquired during heating evolution are presented for experiment #1 and #2 in figure 2 and 3. Each temperature profile is associated with the acquisition time given in the legend even though it was obtained through averaging temperature data acquired for 20 seconds at each thermocouple location.

Three portions characterize each profile. The portion of the profile close to the boundary presents a negative gradient related to the existence of the thermal boundary layer. Then, the profile has a uniform temperature, $\bar{T}(t)$, where the mixing layer is located. Finally, above the mixing region, the temperature profile practically collapses onto the straight line of the initial stratification. The temperature profile in the stable layer is not noticeably affected by the growing mixing layer. This seems to hold even at late stages in the evolution when the velocity data indicate some internal wave activity in the stable layer. Observing profiles relative to the latest time intervals, we found that some cooling occurs at a given point before that local interface reach that point, resulting in a deviation from the original stratification profile that become less stable (the slope increase and so the thermal gradient decrease).

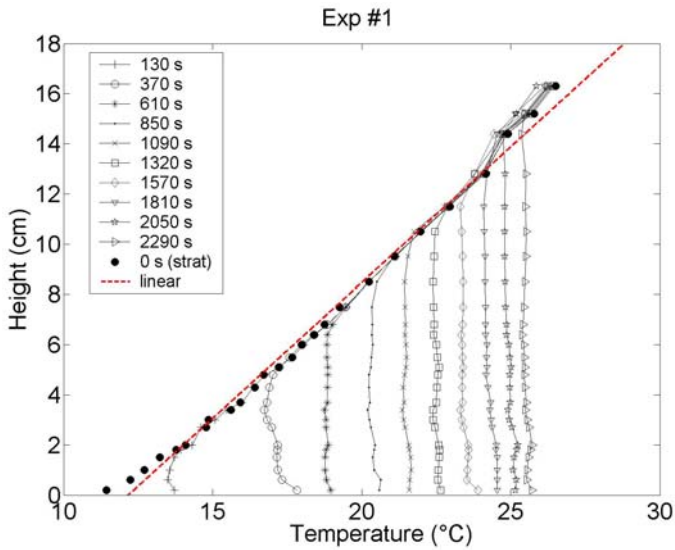


Figure 2 Temperature vertical profiles for experiment #1 (the stratification profile is the one at $t=0$ s)

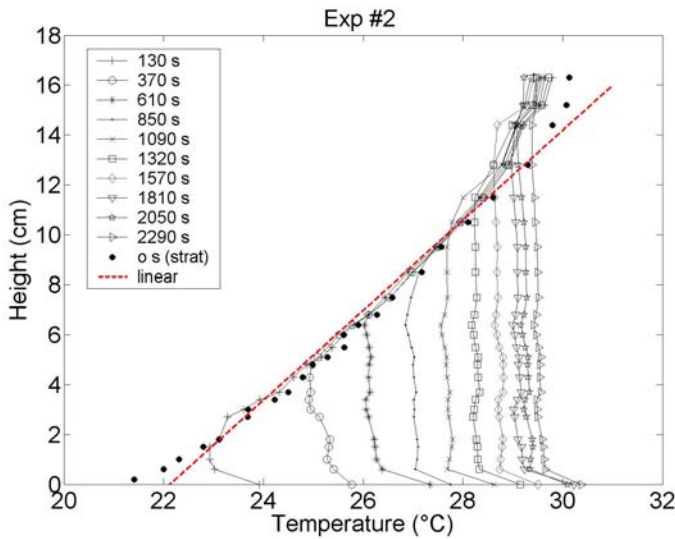


Figure 3 Temperature vertical profiles for experiment #2 (the stratification profile is the one at $t=0$ s)

Figure 4 presents the superimposition of the mixing layer growth profiles detected for exp #1 and #2, employing equation (1). Exp #2 presents a stratification gradient (α) greater than Exp #1 but the final value of the temperature reached at the test section bottom is slightly larger for Exp #1. As a matter of fact, the stratification gradient plays a dominant role in the dynamics of the mixing layer growth. Lower stratification gradients correspond to a greater resistance of the stable layer to be eroded by the plume. In fact, for Exp #1 an heating temperature greater than for Exp #2 is necessary to reach a similar mixing layer growth (even approaching greater value of mixing layer height).

Observing the variance profiles of the velocity vertical component (Figure 5) we can have information about the vertical extension of the mixing region and its evolution. We expect values of the velocity variance larger inside the mixing

region than in the stable layer where it should vanish. According to this expectation profiles have a typical behaviour with a maximum that became larger for longer time and a inflection point moving upward. Subsequently all profiles collapse to values very close to zero.

Each profile presented in figure 5 is compared with the snapshot of feature trajectories relative to the same time. The red profile in the plot is relative to the particular time considered, while the red straight line in the image identifies the height of mixing layer computed from temperature measurements. In particular we notice the mixing region spreads upward; after about 10 minutes, we can also clearly recognize the internal waves in the stable layer and their increasing amplitude with time.

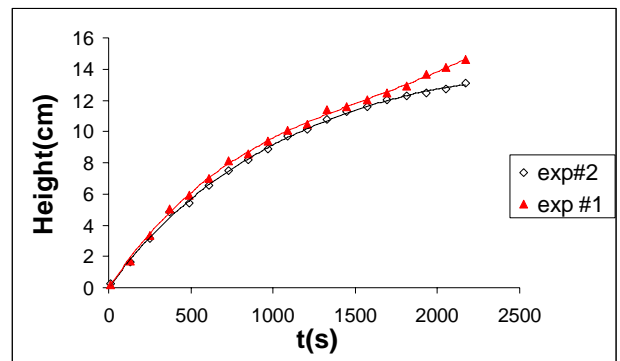


Figure 4 Comparison of mixing layer growth for experiments #1 and #2

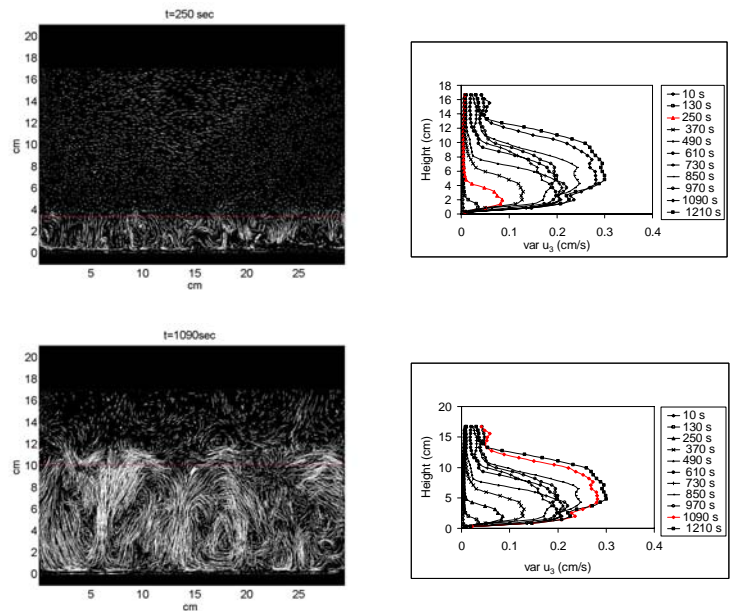


Figure 5. Time evolution of vertical velocity variance profiles compared with mixing layer height evolution derived quantitatively from temperature measurement and qualitatively from trajectories observation (Exp #1).

The region occupied by domes (and so the region interested by higher values of variance) expands a little over the region of temperature homogeneity (pointed by the straight red line in the images). This evidence proves the entrainment phenomenon of the turbulent region inside the stable layer, responsible for the increasing in magnitude of the turbulent structures.

We have computed the spatial autocorrelation function for the horizontal and vertical velocity components within the mixing layer. Velocity vectors belonging to a layer centred at the convective area centreline and 20% of the mixing layer height high are taken into account employing the hypothesis of homogeneity in both the horizontal and vertical directions within the layer taken into account.

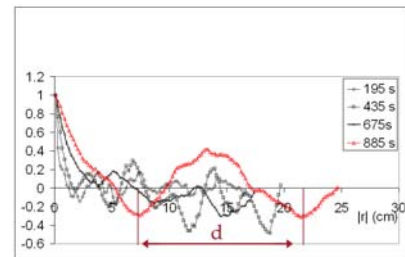
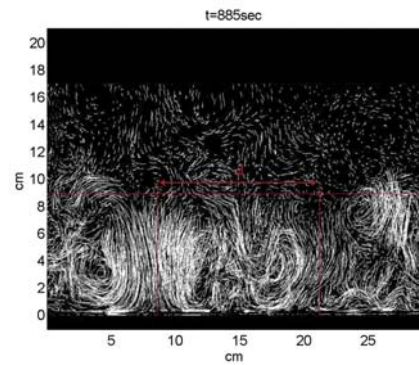
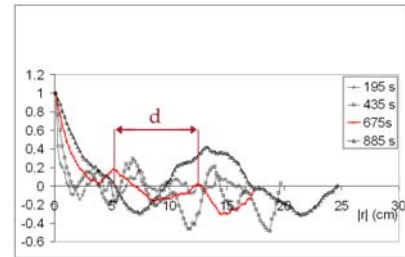
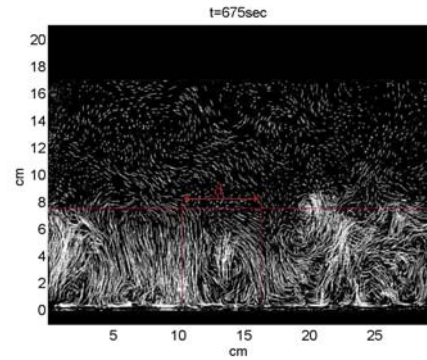
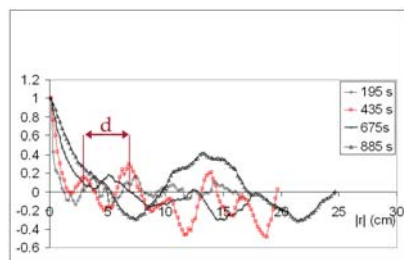
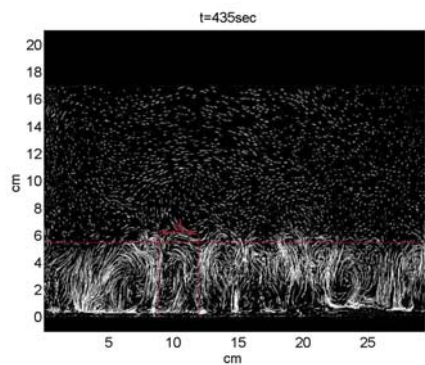
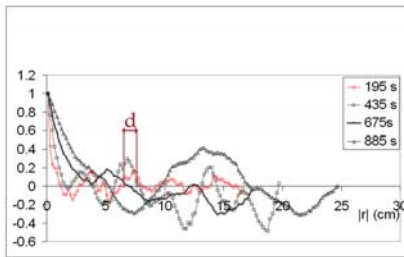
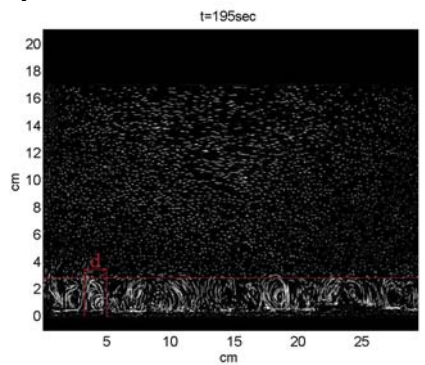


Figure 6 Spatial autocorrelation of the vertical component of the velocity field for four instants of time (exp #1)

Figure 6 presents the spatial correlation of the vertical component of the velocity field for four instants of time. The oscillating behaviour of each line allows the transverse dimension of the plumes within the mixing layer, for a given time the correlation refers to, to be evaluated. The characteristic dimension of the vertical structures increases with time. For small times, the number of velocity samples belonging to the layer within the mixing region taken into account to compute the correlation is inadequate to gather a statistically acceptable result.

The correlation goes toward zero faster for smaller time, this agrees with the fact that structures are expected to be smaller; moreover, the horizontal characteristic dimension of domes increases with time. The distance between two peaks in each plot are compared with the distance between two domes. Notice the results are in a very good agreement for each time instant presented.

CONCLUSION

The flux through the interface between the mixing layer and the stable layer plays a major role in understanding, characterizing and forecasting the quality of water in stratified lakes and in the upper portion of the oceans and the quality of air in the atmosphere. These issues have motivated our experimental investigation that was aimed at predicting mixing layer growth as a function of initial and boundary conditions, understanding the interaction between the mixing layer and the stable layer (e.g., internal waves) and describing the fate of a contaminant dissolved within the fluid phase.

Characteristic structures have been observed in the convective boundary layer: growing domes or turrets presenting an extremely sharp interface at their top, flat regions of large horizontal extent after a dome has spread out or receded, and cusp-shaped regions of entrainment pointing into the convective fluid. Dome characteristic dimensions are of the same order of magnitude as the mixing layer height, while their lifetime is less or equal to the time a fluid particle would need to complete a whole cycle moving through the rising dome and returning in the downwelling region.

There are some phenomena, i.e. pollutant dispersion, that are naturally described in a Lagrangian frame of reference. For a full Lagrangian description, particles have to be tracked for a period of several phenomenon time scales.

The flow under investigation is unsteady in a Lagrangian reference frame since particles, during their motion, reach regions that can be considered homogeneous only in the horizontal plane. The Feature Tracking technique allows long trajectories to be reconstructed within the flow field. As images with a large particle density can be analyzed with FT, the statistics can be more robust than from classical Particle Tracking Velocimetry.

The spatial covariance of the velocity field, providing the plume horizontal dimension, allows the spatial extension of the mixing region to be determined, for a whole individuation of turbulent structures inside the domain.

A more detailed description of non local transport and mixing can be obtained by employing the Transilient Matrix, whose elements contain the fractional tracer concentration moving in a given time interval from a sub-volume to another [17].

REFERENCES

[1] Cenedese A., Dore V., Moroni M., Penetrative convection in stratified fluids: velocity measurements by image analysis techniques, *proceedings of 11th Euromech E.T.C.*, Porto (Portugal) 2007, pp.636-638.
 [2] Cenedese A., Querzoli G., A laboratory model of turbulent convection in the atmospheric boundary layer, *Atmospheric Environment*, Vol. 28, No. 11, 1994, pp. 1901

[3] Cenedese A., Querzoli G., Lagrangian statistics and transilient matrix measurements by PTV in a convective boundary layer, *Meass.Sci.Techonol.*, Vol. 8, 1997, pp. 1553
 [4] Cenedese A., Moroni M., Querzoli G., application of PTV to the study of Penetrative Convection, *10th International Symposium on Flow Visualization. Kyoto (Japan)*, August 2002.
 [5] Cushman J.H., Park M., Kleinfelter N., Moroni M., super diffusion via Lévy lagrangian velocity processes, *Geophys. Res. Letter.*, Vol. 32, 2005, L19816.
 [6] Deardorff J.W., Willis G.E., Lilly D.K., Laboratory investigation of non-steady penetrative convection, *J. Fluid Mech. Vol. 35*, No1, 1969, pp 7-31.
 [7] Deardorff J.W., Convective velocity and temperature scales for the unstable planetary boundary layer and for Rayleigh convection, *J. Atmos. Sci.* Vol.27, 1970, pp.1211-1213.
 [8] Imberger J., Ivey G.N., On the Nature of Turbulence in a Stratified Fluid. Part II: Application to Lakes, *Journal of Physical Oceanography*, Vol.21, 1991,pp. 659-680.
 [9] Jahne B. Digital Image processing. *Springler Verlag*, 1997.
 [10] Kato H., Phillips O.M., On the penetration of a turbulent layer into stratified fluid, *J. Fluid Mech.* Vol.37, No.4, 1969, pp.643.
 [11] Kleinfelter N., Moroni M., Cushman J.H., Application of the finite-size Lyapunov exponent to particle tracking velocimetry in fluid mechanics experiments, *Phys. Rev. E* 72, (2005), 056306.
 [12] Lucas B.D. and Kanade T., An iterative image registration technique with an application to stereo vision, *Proc. Imaging Understanding Workshop* 121-130, 1981.
 [13] Miesch M.S., Brandenburg A., Zweibel E.G., Nonlocal transport of passive scalars in turbulent penetrative convection, *Physical Review E* 61, No.1, 2000, pp. 457-467.
 [14] Miozzi M., Particle Image Velocimetry using Feature Tracking and Delaunay Tessellation, *Proc. 12th International Symposium Application of laser techniques to fluid mechanics*, Lisbon 2004.
 [15] Moroni M., Cushman J.H., Cenedese A., A 3D-PTV Two-projection Study of Pre-asymptotic Dispersion in Porous Media which are Heterogeneous on the Bench Scale, *International Journal of Engineering Science*, Vol.41, No.3-5, 2003, pp.337-370.
 [16] Moroni M., Cenedese A., Comparison among Feature Tracking and More Consolidated Velocimetry Image Analysis Techniques in a Fully Developed Turbulent Channel Flow, *Measurement Science and Technology*, Vol.16, 2005, pp.2307-2322.
 [17] Moroni M., Cenedese A., Penetrative convection in stratified fluids: velocity measurements by image analysis techniques, *Nonlinear process in Geophysics*, Vol.13, 2006, pp. 353-363.
 [18] Querzoli G., A Lagrangian study of particle dispersion in the unstable boundary layer, *Atmospheric Environment*, Vol.30, No.16, 1996, pp. 2821.
 [19] R.B. Stull, An Introduction to Boundary Layer Meteorology, Kluwer, Dordrecht, 1988.
 [20] Tomasi C. and Kanade T., Detection and tracking of point features. Shape and motion from image streams: a factorization method, *Carnegie Mellon University Technical Report CMU-CS-*, 1991, pp.91-132.
 [21] Townsend A.A., Internal waves produced by a convective layer, *J. Fluid Mech.*, Vol.24, No 2, 1964, pp. 307.
 [22] Udrea D.D., Bryanston-Cross P.J., Moroni M. and Querzoli G., Particle Tracking Velocimetry techniques *Fluid Mechanics and its Application* Kluwer Academic (The Netherlands), 2000, pp.279-304